



Target effects on electrical properties and laser induced voltages of $\text{La}_{0.72}\text{Ca}_{0.28}\text{MnO}_3$ thin films prepared by pulsed laser deposition

Hui ZHANG, Wen-zhang WANG, Qi CUI, Dong YE, Ji MA, Qing-ming CHEN, Xiang LIU

Faculty of Materials Science and Engineering, Kunming University of Science and Technology,
Kunming 650093, China

Received 8 January 2014; accepted 10 April 2014

Abstract: $\text{La}_{0.72}\text{Ca}_{0.28}\text{MnO}_3$ thin films were deposited on untilted and 15° tilted LaAlO_3 (100) single crystalline substrates by pulsed laser deposition. The polycrystalline targets used in the deposition process were synthesized by sol–gel and coprecipitation methods, respectively. The structure, electrical transport properties and surface morphology of the targets and films were studied. It is found that, compared with coprecipitation method, the sol–gel target has more homogeneous components and larger density and grain size, thus the higher insulator–metal transition temperature and larger temperature coefficient of resistivity. The thin film prepared by sol–gel target has a uniform grain size and higher quality. The metal–insulator transition temperature is higher and the laser induced voltage signal is larger. Preparing the target by sol–gel method can largely improve the properties of corresponding thin films in pulsed laser deposition process.

Key words: $\text{La}_{0.72}\text{Ca}_{0.28}\text{MnO}_3$; target; thin film; sol–gel method; coprecipitation method

1 Introduction

Mixed-valence manganese oxides $\text{La}_{1-x}\text{A}_x\text{MnO}_3$ (A represents the divalent alkaline earth) have been widely studied since they exhibited rich properties such as colossal magnetoresistance (CMR), metal-insulator transition, phase separation and charge ordering [1–4]. A lot of experimental and theoretical research results about this material system have been reported since the CMR effect was discovered [5–7]. The double exchange (DE) mechanism has been proposed by ZENER [8] to explain the coexistence of ferromagnetic and metallic state. Jahn–Teller distortion is thought to play an important role in determining the magnetic and electronic properties [9]. But they cannot completely explain the CMR effect. Among the manganese oxides, $\text{La}_{1-x}\text{Ca}_x\text{MnO}_3$ is a very interesting system. With the variation of Ca doping level, $\text{La}_{1-x}\text{Ca}_x\text{MnO}_3$ shows a rich phase diagram with a various of ground states, including ferromagnetic metallic (FM), anti-ferromagnetic (AF) insulator, charge ordered (CO) insulator and paramagnetic insulator (PI) states [10]. For $0.25 < x < 0.33$,

$\text{La}_{1-x}\text{Ca}_x\text{MnO}_3$ undergoes a metal–insulator transition at T_p which is close to the ferromagnetic to paramagnetic transition temperature T_C [5].

Many methods such as solid state reaction [11], sol–gel [12,13] and chemical solution approach [14] have been employed to synthesize the $\text{La}_{1-x}\text{Ca}_x\text{MnO}_3$ polycrystalline. Metal-organic deposition [15] and pulsed laser deposition (PLD) are usually used to prepare the $\text{La}_{1-x}\text{Ca}_x\text{MnO}_3$ thin films [16,17]. Previous reports show that the particle size and grain boundary strongly influence the properties of bulk materials [12,18,19]. In terms of thin films, the physical properties are usually quite different from the bulk compounds, since the properties of thin films are very sensitive to strain, oxygen, disorder and deposition parameters [20–23]. For the PLD technique, the quality of the ceramic target is an important factor which determines the properties of film, because its density and homogeneity largely influence the quality of the deposited thin film. However, few researches have focused on the effects of target. In this work, two kinds of $\text{La}_{0.72}\text{Ca}_{0.28}\text{MnO}_3$ targets were synthesized: the sol–gel target and the coprecipitation target (prepared by sol–gel and coprecipitation methods,

respectively). Subsequently, the related thin films were prepared by PLD. The electrical properties, micrographs and laser induced voltage (LIV, the electric voltage is produced through the Seebeck effect when a temperature gradient is generated by pulsed laser radiation between the top and bottom of the films) of the films were studied.

2 Experimental

The $\text{La}_{0.72}\text{Ca}_{0.28}\text{MnO}_3$ (LCMO) precursor powders were synthesized by sol-gel and coprecipitation methods, respectively. The details of the process can be found in our previous works [24,25]. The powders were first calcined at 550 °C for 16 h. Then, the obtained black powders were ground and pressed into disk pellet, and then sintered at 1150 °C for 16 h in air. The samples were named as S1 and C1, respectively. Using these ceramic targets, $\text{La}_{0.72}\text{Ca}_{0.28}\text{MnO}_3$ thin films with the thickness about 200 nm were deposited on untilted (0°) and 15° tilted LaAlO_3 (100) substrates by pulsed laser deposition. The films were grown at 790 °C in 100 Pa oxygen pressure and annealed at 760 °C in oxygen pressure of 3×10^4 Pa for 30 min. The thin films were labeled as S0 (prepared by sol-gel target on 0° LAO substrate), S15, C0 and C15, respectively.

The crystallinity of targets and films was examined by X-ray diffraction (XRD) with θ - 2θ scan. The surface morphologies of the targets and films were characterized by scanning electron microscopy (SEM) and atomic force microscopy (AFM), respectively. The temperature dependence of resistance of the samples was measured by the four-probe method at the temperature of 300 to 100 K. For the measurement of LIV signals, two indium electrodes separated about 1 mm were placed on the surface of the films [26]. The films were irradiated by a pulse laser with 248 nm in wavelength and 28 ns in duration. The signal was monitored with an oscilloscope (Tektronix TDS2022B) at room temperature.

3 Results and discussion

3.1 Properties of targets

Figure 1 shows the XRD patterns of the $\text{La}_{0.72}\text{Ca}_{0.28}\text{MnO}_3$ targets synthesized by sol-gel and coprecipitation methods. Both the samples possess single phase without any detectable impurities. Figure 2 shows the typical ρ - T curves of S1 and C1. An evident difference that the metal-insulator transition region is broad for C1 and narrow for S1 can be seen. The broadening behavior of the coprecipitation sample can be attributed to the inhomogeneity of the ceramic prepared by coprecipitation method. In addition, C1 has a slight shoulder in the metal region, which also indicates the

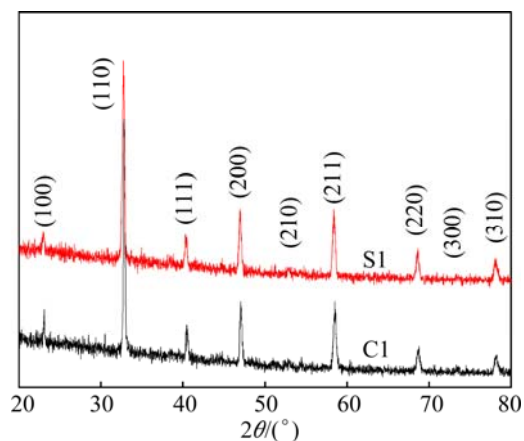


Fig. 1 XRD patterns of LCMO targets

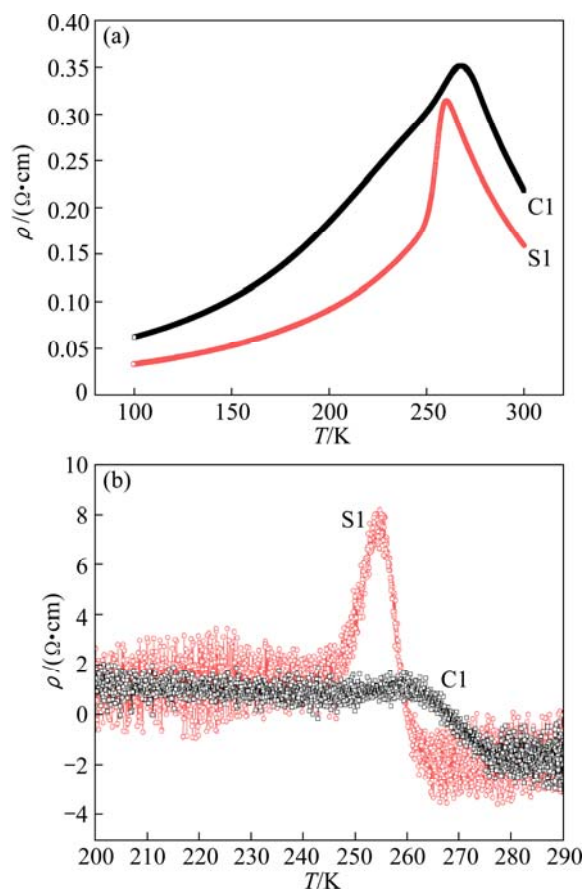


Fig. 2 Temperature dependence of resistivity (a) and TCR curves of LCMO targets (b)

inhomogeneity of the coprecipitation sample. As a consequence, the temperature coefficient of resistivity (TCR) ($\text{TCR} = (d\rho/dT)\rho^{-1} \times 100\%$) of S1 (8.0%) is much larger than that of C1 (1.6%) (Fig. 2(b)). It is well known that the sol-gel method produces samples with very uniform particles and precise components. It can be seen from Fig. 3 that the micrographs of C1 and S1 are very different. There are many small grains (~ 400 nm) and

pores among the large grains ($\sim 1 \mu\text{m}$) in sample C1, indicating the existence of a large number of grain boundaries and a possible phase inhomogeneity. It may be due to the relatively large particle size and irregular shape of the coprecipitation powders [24]. As for sample S1, the size and shape of powder particles are more uniform, so the grains grow more quickly, and are larger ($1\sim 2 \mu\text{m}$), and more uniform, and the sample is denser. So, the phase of the sol-gel sample is more homogeneous and the electrical transport property is better. Therefore, sample S1 has higher metal-insulator transition temperature (T_p) and TCR values, which are summarized in Table 1.

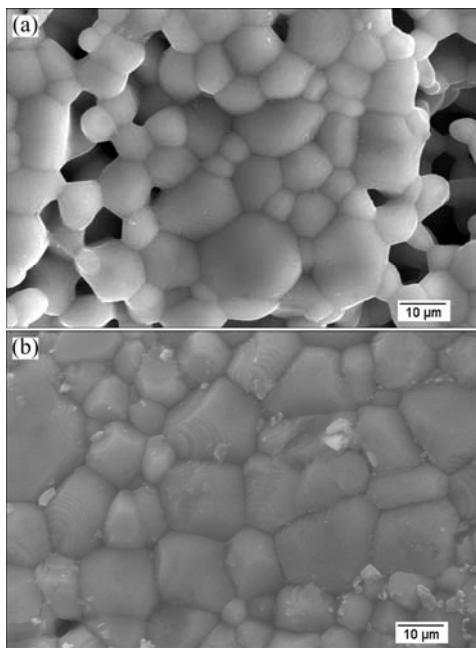


Fig. 3 SEM images of LCMO targets of C1 (a) and S1 (b)

Table 1 Experimental data of LCMO targets and thin films

Sample	T_p/K	TCR/%	U_p/V
C1	267.6	1.6	–
S1	260.0	8.0	–
C0	248.2	9.2	–
C15	243.1	8.4	1.5
S0	263.3	8.0	–
S15	266.5	7.8	2.2

3.2 Properties of films

In Fig. 4, the XRD patterns of LCMO films grown on 0° and 15° LaAlO_3 (LAO) substrates are given. It can be seen that only (100) reflection peaks of the films appear, indicating that the films have a single phase and can be indexed based on the single perovskite unit cell. Film S0 shows a double (200) reflection peak structure, implying a possible double growth orientation, which may be induced by the lattice and strain relaxation. The

thin films grown on the tilted substrate (S15 and C15) have lower peak intensity, which is due to the difficulty in growing high quality film on the substrate with high tilting angle [26].

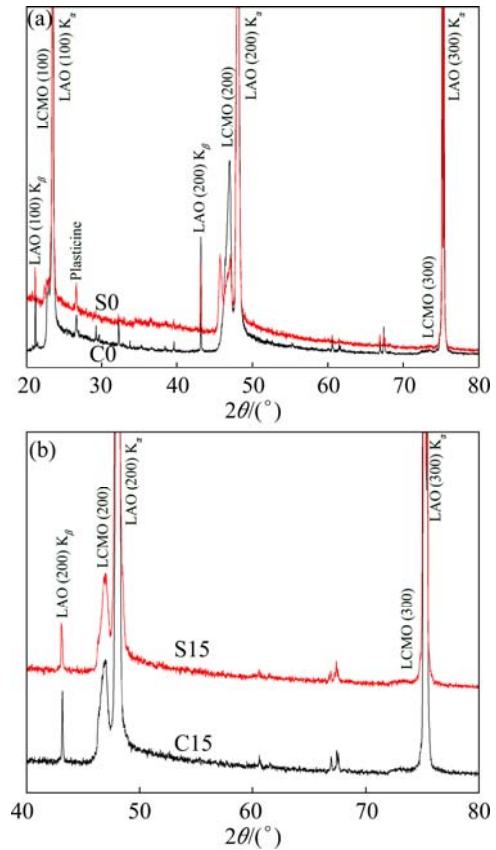


Fig. 4 XRD patterns of LCMO films grown on 0° (a) and 15° (b) substrates by sol-gel and coprecipitation targets

The AFM images of C15 and S15 are shown in Fig. 5 and a layer-structure surface can be observed. S15 has a more uniform and smaller grain size which distributes between 80–100 nm. Most of the grains of C15 are agglomerated and the grain size distributes between 200–300 nm. The surface roughness of C15 is also larger than that of S1, which is in agreement with the quality of targets. Since the sol-gel target is more homogeneous and has larger grains, it is favorable to obtaining high quality film with uniform grain size and smooth surface during the PLD deposition process. By contrast, the coprecipitation target surface has more pores, which will influence the plasma shape and size, and hence the thickness uniform of thin film. The inhomogeneity of coprecipitation target will induce the roughness and agglomerate of corresponding film.

Figure 6 shows the temperature dependence of resistance ($R(T)/R(297 \text{ K})$) and TCR curves of the films. T_p of coprecipitation thin films (C0 and C15) and sol-gel thin films (S0 and S15) are around 245 K and 265 K, respectively. This is attributed to the inhomogeneity and

larger surface roughness of the coprecipitation films. TCR of the 0° films (C0 and S0) is a little larger than that of 15° films, which may be explained by the low quality of films grown on the substrate with high tilting angle [26]. The large roughness and low quality of film will increase the resistivity and reduce the T_p value through decreasing the electron hopping [27]. As for the application of bolometer, high insulator–metal transition

temperature and large TCR values are important. So, it can be concluded that the sol–gel method can produce higher quality target, which can be used to prepare higher quality thin film with better electrical transport properties.

The target effects on the laser induced voltage signals of films are shown in Fig. 7. The energy density of the incident laser was changed from 0.1 to 0.6

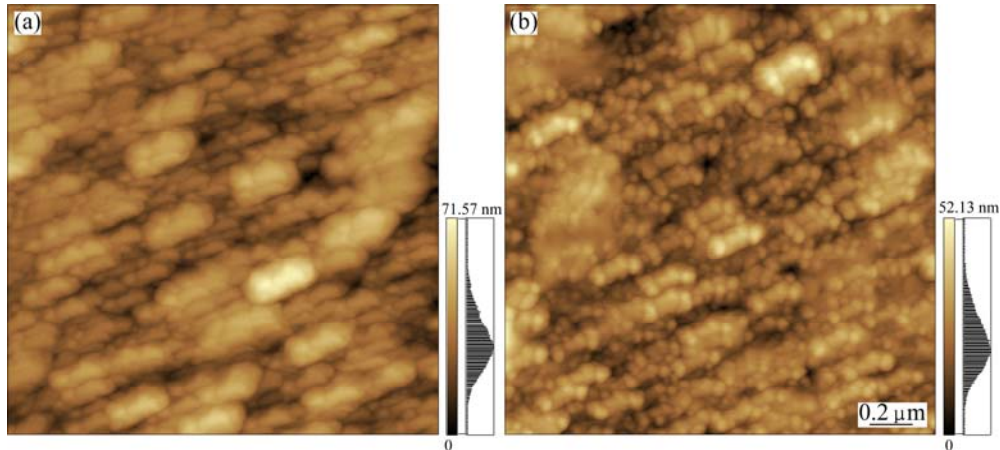


Fig. 5 AFM images of LCMO films grown on 15° tilted LAO substrates: (a) C15; (b) S15

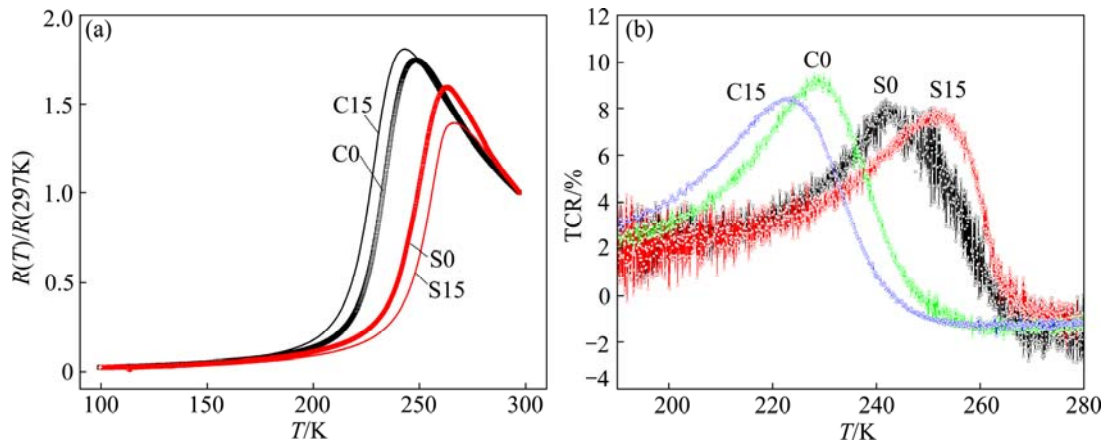


Fig. 6 Temperature dependence of resistance (a) and TCR curves of LCMO thin films (b)

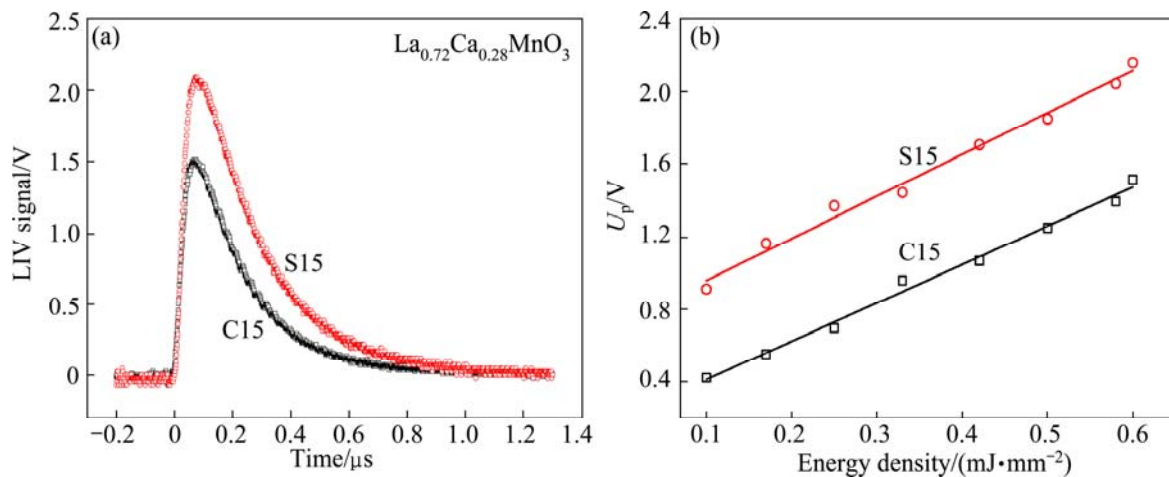


Fig. 7 LIV signals of 15° tilted LCMO films (a) and liner relationship between peak voltages and energy density (b)

mJ/mm². According to the atomic layer thermopile model proposed by LENGFELLNER et al [28], the induced voltage is mainly determined by the Seebeck coefficient anisotropy ΔS , which includes the structural and electrical transport anisotropy [29]. As can be seen in Fig. 7(a), the peak voltage (U_p) of S15 (2.2 V) is obviously larger than that of C15 (1.5 V), indicating that S15 has a larger ΔS . We think that the inhomogeneity and rough surface of film C15, which were induced by the inhomogeneity and large amount of grain boundaries and pores of target C1, decrease the structural and electrical transport anisotropy and hence lead to a smaller induced voltage. The peak voltage as a function of the incident laser energy density displays a linear relationship, as shown in Fig. 7(b). These results suggest that the thin film prepared by the sol–gel target has a more promising potential application to be used as thermoelectric detector due to its higher T_p and larger U_p . This demonstrates that samples produced with sol–gel method have better physical properties compared with coprecipitation method.

4 Conclusions

1) Both the sol–gel and coprecipitation targets have a single phase after sintering under the same conditions. Compared with the coprecipitation target, the sol–gel target has a narrower insulator–metal transition region and larger temperature coefficient of resistivity.

2) All the thin films deposited with different targets and different LAO substrates grow along *c*-axis and have a single phase. The film prepared by sol–gel target has a more uniform and smaller grain size, and smoother surface.

3) Compared with coprecipitation target the insulator–metal transition temperature of thin films prepared with sol–gel target is higher 20 K, and the laser induced voltage signal is also larger.

4) Target quality heavily influences the film properties. Sol–gel method obviously is a better process to improve the properties of both ceramic target and thin film, and the performance of potential novel devices, such as bolometer and thermoelectric devices.

Acknowledgement

The authors would like to thank Zhi-zheng ZHANG for SEM measurements.

References

[1] LI Ting-xian, ZHANG Fei-peng, FANG Hui, LI Kuo-she, YU Feng-jun. The magnetoelectric properties of $\text{La}_{0.7}\text{Sr}_{0.3}\text{MnO}_3/\text{BaTiO}_3$ bilayers with various orientations [J]. *Journal of Alloys and Compounds*, 2013, 560: 167–170.

[2] ZHOU Zheng-you, WU Xiao-shan, LUO Guang-sheng, JIANG

Feng-yi. Effect of second introduced phase on magnetotransport properties of $\text{La}_{2/3}\text{Sr}_{1/3}\text{MnO}_3/0.33(\text{CuO}, \text{ZnO}, \text{Al}_2\text{O}_3)$ composites [J]. *Transactions of Nonferrous Metals Society of China*, 2008, 18(4): 890–896.

[3] RAHMOUNI H, CHERIF B, BAAZAOUI M, KHIROUNI K. Effects of iron concentrations on the electrical properties of $\text{La}_{0.67}\text{Ba}_{0.33}\text{Mn}_{1-x}\text{Fe}_x\text{O}_3$ [J]. *Journal of Alloys and Compounds*, 2013, 575: 5–9.

[4] LUO Guang-sheng, LIU Guang-hua, LI Xiao-yi, XIONG Wei-hao, WU Xiao-shan. Structure and transport properties of $(\text{La}_{(1-x-y)}\text{Y}_{(y)})_{(2/3)}\text{Ca}_{1/3}\text{MnO}_3$ with La-site vacancies [J]. *Transactions of Nonferrous Metals Society of China*, 2007, 17(5): 992–995.

[5] OKUDA T, TOMIOKA Y, ASAMITSU A, TOKURA Y. Low-temperature properties of $\text{La}_{1-x}\text{Ca}_x\text{MnO}_3$ single crystals: Comparison with $\text{La}_{1-x}\text{Sr}_x\text{MnO}_3$ [J]. *Physical Review B*, 2000, 61(12): 8009–8015.

[6] FENG Jin, XIAO Bin, ZHOU Rong, PAN Wei. Electronic and magnetic properties of double perovskite slab–rocksalt layer rare earth strontium aluminates natural superlattice structure [J]. *Journal of Applied Physics*, 2013, 113: 143907-1–10.

[7] FENG J, XIAO B, WAN C L, QU Z X, HUANF Z C, CHEN J C, ZHOU R, PAN W. Electronic structure, mechanical properties and thermal conductivity of $\text{Ln}_2\text{Zr}_2\text{O}_7$ (Ln=La, Pr, Nd, Sm, Eu and Gd) pyrochlore [J]. *Acta Materialia*, 2011, 59(4): 1742–1760.

[8] ZENER C. Interaction between the d-shells in the transition metals. II. Ferromagnetic compounds of manganese with perovskite structure [J]. *Physical Review*, 1951, 82(3): 403–405.

[9] MILLIS A J, SHRAIMAN B I, MUELLER R. Dynamic Jahn–Teller effect and colossal magnetoresistance in $\text{La}_{1-x}\text{Sr}_x\text{MnO}_3$ [J]. *Physical Review Letters*, 1996, 77(1): 175–178.

[10] CHEONG S W, AND HWANG H Y. In colossal magnetoresistive oxides [M]. New York: Gordon and Breach Science Publishers, 2000.

[11] KUMAR N, KISHAN H, RAO A, AWANA V P S. Structural, electrical, magnetic, and thermal studies of Cr-doped $\text{La}_{0.7}\text{Ca}_{0.3}\text{Mn}_{1-x}\text{Cr}_x\text{O}_3$ ($0 \leq x \leq 1$) manganites [J]. *Journal of Applied Physics*, 2010, 107: 083905-1–6.

[12] KUBERKAR D G, DOSHI R R, SOLANKI P S, KHACHAR U, VAGADIA M, RAVALIA A, GANESAN V. Grain morphology and size disorder effect on the transport and magnetotransport in sol–gel grown nanostructured manganites [J]. *Applied Surface Science*, 2012, 258(22): 9041–9046.

[13] ZHOU S M, ZHAO S Y, HE L F, GUO Y Q, SHI L. Facile synthesis of Ca-doped manganite nanoparticles by a nonaqueous sol–gel method and their magnetic properties [J]. *Materials Chemistry and Physics*, 2010, 120(1): 75–78.

[14] FEI Ling, ZHU Le-yi, CHENG Xue-mei, WANG Hai-yan, BABER S M, HILL J, LIN Qiang-lu, XU Yun, DENG Shu-guang, LUO Hong-mei. Structure and magnetotransport properties of epitaxial nanocomposite $\text{La}_{0.67}\text{Ca}_{0.33}\text{MnO}_3:\text{SrTiO}_3$ thin films grown by a chemical solution approach [J]. *Applied Physics Letters*, 2012, 100: 082403-1–5.

[15] DAOUDI K, TSUCHIYA T, YAMAGUCHI I, MANABE T, MIZUTA S, KUMAGAI T. Microstructural and electrical properties of $\text{La}_{0.7}\text{Ca}_{0.3}\text{MnO}_3$ thin films grown on SrTiO_3 and LaAlO_3 substrates using metal–organic deposition [J]. *Journal of Applied Physics*, 2005, 98: 013507: 1–6.

[16] DEBNATH J C, KIM J H, HEO Y, STRYDOM A M, AND DOU S X. Correlation between structural parameters and the magnetocaloric effect in epitaxial $\text{La}_{0.8}\text{Ca}_{0.2}\text{MnO}_3/\text{LaAlO}_3$ thin film [J]. *Journal of Applied Physics*, 2013, 113: 063508-1–6.

[17] HEINZE S, HABERMEIER H U, CRISTIANI G, BLANCO CANOSA S, LE TACON M, KEIMER B. Thermoelectric properties of $\text{YBa}_2\text{Cu}_3\text{O}_{7-\delta}-\text{La}_{2/3}\text{Ca}_{1/3}\text{MnO}_3$ superlattices [J]. *Applied Physics Letters*, 2012, 101: 131603-1–4.

- [18] DONG Shuai, YU Rong, YUNOKI S, LIU J M, DAGOTTO E. Ferromagnetic tendency at the surface of CE-type charge-ordered manganites [J]. *Physical Review B*, 2008, 78(6): 064414-1–7.
- [19] DEY P, NATH T K, MANNA P K, YUSUF S M. Enhanced grain surface effect on magnetic properties of nanometric $\text{La}_{0.7}\text{Ca}_{0.3}\text{MnO}_3$ manganite: Evidence of surface spin freezing of manganite nanoparticles [J]. *Journal of Applied Physics*, 2008, 104: 103907-1–12.
- [20] HAN Yun-xin, WU Wen-bin, JIANG Guo-shun, ZHU Chang-fei. Annealing induced coherent evolutions of biaxial strain and antiferromagnetic-insulator phase in $\text{La}_{0.625}\text{Ca}_{0.375}\text{MnO}_3$ films [J]. *Journal of Applied Physics*, 2012, 112: 063716-1–5.
- [21] MA Ji, ZHANG Hui, CHEN Qing-ming, LIU Xiang. Effects of substrate-induced-strain on the electrical properties and laser induced voltages of tilted $\text{La}_{0.67}\text{Ca}_{0.33}\text{MnO}_3$ thin films [J]. *Journal of Applied Physics*, 2013, 114: 043708-1–5.
- [22] BITLA Y, KAUL S N. Effect of oxygen off-stoichiometry on magnetic and magneto-transport properties of nanocrystalline under-doped LCMO [J]. *Journal of Applied Physics*, 2012, 111: 07D717-1–3.
- [23] AYDOGDUA G H, KURUA Y, NELAYAHB J, van AKENB P A, HABERMEIER H U. Thickness dependent microstructural changes in $\text{La}_{0.5}\text{Ca}_{0.5}\text{MnO}_3$ thin films deposited on (111) SrTiO_3 [J]. *Thin Solid Films*, 2010, 518(16): 4667–4669.
- [24] MA Ji, THEINGI M, CHEN Qing-ming, WANG Wen-zhang, LIU Xiang, ZHANG Hui. Influence of synthesis methods and calcination temperature on electrical properties of $\text{La}_{1-x}\text{Ca}_x\text{MnO}_3$ ($x=0.33$ and 0.28) ceramics [J]. *Ceramics International*, 2013, 39: 7839–7843.
- [25] THEINGI M, MA Ji, ZHANG Hui, WANG Wen-zhang, YI Jian-hong, CHEN Qing-ming. Synthesis and characterization of nanocrystalline $\text{La}_{0.67}\text{Ca}_{0.33}\text{MnO}_3$ powder by a simple sol–gel method [J]. *Journal of Synthetic Crystals*, 2013, 42(2): 345–350.
- [26] ZHANG P X, HABERMEIER H U. Atomic layer thermopile materials: Physics and application [J]. *Journal of Nanomaterials* 2008, 2008: 329601-1–12.
- [27] SALVATO M, VECCHIONE A, de SANTIS A, BOBBA F, CUCOLO A M. Metal-insulator transition temperature enhancement in $\text{La}_{0.7}\text{Ca}_{0.3}\text{MnO}_3$ thin films [J]. *Journal of Applied Physics*, 2005, 97: 103712-1–5.
- [28] LENGFELLNER H, KREMB G, SCHNELLBÖGL A, BETZ J, RENK K F, PRETTL W. Giant voltages upon surface heating in normal $\text{YBa}_2\text{Cu}_3\text{O}_{7-\delta}$ films suggesting an atomic layer thermopile [J]. *Applied Physics Letters*, 1992, 60: 501: 1–3.
- [29] LI X H, HABERMEIER H U, ZHANG P X. Laser-induced off-diagonal thermoelectric voltage in $\text{La}_{1-x}\text{Ca}_x\text{MnO}_3$ thin films [J]. *Journal of Magnetism and Magnetic Materials*, 2000, 211(1–3): 232–237.

脉冲激光沉积镀膜工艺中不同靶材制备方法对 $\text{La}_{0.72}\text{Ca}_{0.28}\text{MnO}_3$ 薄膜电学性能和激光感生电压的影响

张辉, 王文章, 崔琦, 业冬, 马吉, 陈清明, 刘翔

昆明理工大学 材料科学与工程学院, 昆明 650093

摘要: 采用脉冲激光沉积方法在单晶 LaAlO_3 (100)平衬底和 15° 倾斜衬底上制备 $\text{La}_{0.72}\text{Ca}_{0.28}\text{MnO}_3$ 薄膜。在镀膜过程中分别采用溶胶–凝胶法和共沉淀法制备靶材。研究不同方法制备的靶材和相应的薄膜的结构、电输运性能和表面形貌。与共沉淀法相比, 采用溶胶–凝胶法制备的靶材具有更加均匀的组分和更大的致密度以及晶粒尺寸, 因此具有更高的绝缘体–金属转变温度和更大的电阻温度系数。采用溶胶–凝胶靶材制备的薄膜, 其晶粒尺寸更均匀、生长质量更好, 绝缘体–金属转变温度高 20 K, 激光感生电压也更大。因此, 使用溶胶–凝胶方法制备靶材可以大幅提高脉冲激光沉积方法中薄膜的性能。

关键词: $\text{La}_{0.72}\text{Ca}_{0.28}\text{MnO}_3$; 靶材; 薄膜; 溶胶–凝胶法; 共沉淀法

(Edited by Xiang-qun LI)